J Mater Sci (2012) 47:754–763
DOI 10.1007/s10853-011-5851-7

Synthesis and cytocompatibility of manganese (II) and iron (III) substituted hydroxyapatite nanoparticles

Yan Li · Jasmine Widodo · Sierin Lim · Chui Ping Ooi

Received: 13 May 2011 / Accepted: 3 August 2011 / Published online: 23 August 2011

Abstract Manganese (II) and iron (III) substituted hydroxyapatite (HA, $Ca_{10}(PO_4)_6(OH)_2$) nanoparticles were synthesized using wet chemical method. All samples were single-phase, non-stoichiometric and B-type carbonated hydroxyapatite. Compared with pure HA, Mn^{2+} substituted (MnHA) and Fe^{3+} doped HA (FeHA) did not demonstrate significant structure deviation. Since ion exchange mechanism was applied for the synthesis process, the morphology and particle size were not significantly affected: all samples were elongated spheroids of around 70 nm. The presence of Fe and Mn was confirmed by energy dispersive X-ray spectroscopy (EDX) while the concentrations were quantified by inductively coupled plasma (ICP). Fe^{3+} ions were more active than Mn^{2+} ions in replacing Ca^{2+} ions in HA lattice structure. The magnetic property of HA was modified by substitution with Fe. The Fe5 ($Fe_{added}/Ca_{added} = 5\%$ by molar ratio) was paramagnetic while pure HA was diamagnetic. Results of extraction assay from cells cultured in extracted medium for 72 h suggested that both MnHA and FeHA were non-cytotoxic to osteoblast cells. Meanwhile, the presence of Fe^{3+} ions in HA demonstrated significant positive effect on osteoblast cells, where the cell number on Fe5 pellets was twice that of pure HA and MnHA samples.

Y. Li · J. Widodo · S. Lim (✉) · C. P. Ooi (✉)
Division of Bioengineering, School of Chemical and Biomedical Engineering, Nanyang Technological University,
70 Nanyang Dr., Block N1.3, Singapore 637457, Singapore
e-mail: SLim@ntu.edu.sg

C. P. Ooi
e-mail: CPOoi@unisim.edu.sg

Present Address:
C. P. Ooi
School of Science and Technology, SIM University,
Singapore 599490, Singapore

Introduction

Calcium hydroxyapatite is the main inorganic component of natural bones. It is osteoconductive, supporting the bone formation directly on its surface. However, due to the inferior mechanical characteristics, HA is limited to low load bearing applications [1] and has been used as coating material on metallic implants, such as Ti6Al4V [2]. HA coated implants promote osteointegration that enhances tight-fit fixation and reduces motion damages to surrounding tissues [3–5]. Hence, the adhesion of osteoblast to HA coating is a crucial step for subsequent osteoblast functions.

Since Mn^{2+} ions increase ligand binding affinity of integrin and activate cell adhesion, MnHA has attracted great interest for its potential in increasing osteoblast adhesion [6]. MnHA had been successfully synthesized using wet chemical method, as reported by Mayer [6] and György [7]. In the work carried out by György, powder containing 0.55% Mn^{2+} and 2.8% carbonate was chosen as the coating material on Ti substrates. It was found that the proliferation of osteoblasts on MnHA coated Ti surface was enhanced as compared to uncoated Ti surface [7]. However, the relationship between Mn content in HA and the response of osteoblast is still unknown.

Adherence and differentiation of osteoblasts (indicated by alkaline phosphatase synthesis) have been reported to occur at earlier time points for HA doped with trivalent cations (La^{3+}, Y^{3+}, In^{3+} and Bi^{3+}) compared to HA substituted with divalent cations (Mg^{2+} and Zn^{2+}) and pure

HA [8]. Contradictory results on the effect of Fe ions on bone formations in vitro have been reported [9–11] although iron is a vital element for the survival of human beings [12]. Parelman et al. [9] showed that iron restriction by chelator deferoxamine (DFO) impaired mineralization of osteoblasts while both Sato [10] and Takeuchi [11] reported the inhibitory effects of Fe^{3+} on bone formation in vitro. The Fe source used by Sato was saccharated ferric (III) oxide and Takeuchi et al. had used ferric nitrilotriacetate (Fe^{3+}-NTA); while the tests were carried out with solutions of Fe ions in the culture medium. To date, the response of osteoblasts to Fe ions (both Fe^{2+} and Fe^{3+}) in HA (Fe doped HA) is however unknown. In genetic hemochromatosis, iron overload can lead to bone loss [12], meanwhile marginal iron restriction diet on weanling female rats decreased whole-body bone mineral content [9]. Furthermore, Wu et al. [13] reported that Fe^{2+} substituted HA nanoparticles were superparamagnetic and showed good biocompatibility. Hence, it would be of great interest to synthesize FeHA and investigate the growth of osteoblast on FeHA. The Fe-doped HA may demonstrate better biocompatibility than pure HA and benefit the exploration of Fe role on bone metabolism.

To reduce factors affecting cell response, wet chemical method coupled with ion exchange mechanism was used to produce MnHA and FeHA. As reported by Wakamura, FeHA produced by coprecipitation method resulted in larger crystal size than pure HA [14]. Nanophase HA (grain size less than 100 nm) demonstrated better biocompatibility than conventional HA (grain size larger than 100 nm) [15]. Although coprecipitation mechanism usually gives homogenous distribution of metal ion through HA nanoparticles [16], the pH of reaction solution is usually higher than 7.0 and Mn^{2+} ions are oxidized to higher valence at pH 5.8–6.0 [6]. Since coprecipitation method may result in larger crystal size and higher metal ion valence, we chose ion exchange mechanism to fabricate metal ion doped HA nanoparticles with similar morphology and size. All samples were characterized by X-ray diffractometer (XRD), Fourier transform infrared spectroscopy (FTIR), field emission scanning electron microscope (FESEM) coupled with energy dispersive X-ray spectroscopy (EDX) and inductively coupled plasma (ICP). The magnetic property of FeHA was tested using vibrating sample magnetometer (VSM) as superparamagnetic nanoparticles had potential applications in biomedical field such as targeted delivery using external magnetic field or as contrast agent in magnetic resonance imaging. Cytotoxicity test for all samples were performed on osteoblasts by extraction assay. Osteoblasts were further seeded on MnHA and FeHA pellets for 3 and 7 days to investigate the proliferation profiles.

Materials and methods

Synthesis of metal ion doped HA

$Ca(OH)_2$ (3.71 g; Greenrich Chemical Enterprise, 96.0 wt% pure with less than 4% $CaCO_3$) was first stabilized in 250 mL DI water (Mili-Q unit from Milipore) at 98.5 °C and stirred at 500 rpm for 30 min. H_3PO_4 (2 mL 85 wt%; Merck) was diluted into 250 mL DI water and then added into the $Ca(OH)_2$ suspension at 4 mL/min until the pH of mixture had decreased to 5.5 (for MnHA) and 5.0 (for FeHA). After the addition of H_3PO_4 was stopped, metal salt ($MnCl_2{\cdot}4H_2O$ (Riedel-de Haën) (0.099 g, 0.495 g or 0.990 g) or $FeCl_3{\cdot}6H_2O$ (Sigma-Aldrich) (0.135 g or 0.676 g)) in solution was added to the mixture. The pH was maintained at 5.5 (for MnHA) and 5.0 for FeHA with NH_4OH. The mixture was stirred at 500 rpm at 98.5 °C for 2 h and left to settle overnight. The settled precipitate was washed three times with DI water, dried at 100 °C overnight and ground to powder for further characterization. The samples were labelled as MX (where X was defined as the molar percentage or atomic ratio of added metal ion to added Ca).

Characterization techniques

Metal ion doped HA was characterized by the following techniques, XRD, FTIR, FESEM with EDX, and ICP. For FeHA, magnetic property was tested by VSM.

XRD characterization

Bruker D8 Advance X-ray diffractometer with Cu-Kα radiation at 40 kV and 40 mA was used for phase analysis. Data was collected at a step size of 0.04 degree and counting time of 15 s per step in a 2θ range of 20–80°. The lattice parameters a and c were calculated based on the XRD patterns using the program TOPAS 2.1 (Bruker) with the starting structure of a hexagonal model with space group $P6_3/m$ as reported by Sudarsanan and Young [17]. The crystal size was tabulated using Scherrer equation [18]:

$$d = \frac{k\lambda}{B_{1/2}\cos\theta} \quad (1)$$

where, d is the crystal size, k is the shape coefficient and is 0.9 for elongated apatite crystallites, λ is the wavelength of Cu-Kα radiation (1.540980 Å) and $B_{1/2}$ (rad) is the full width at half maximum intensity (FWHM) of peak belonging to (002) plane.

FTIR characterization

The functional groups of samples were investigated by FTIR spectroscopy (PerkinElmer, Spectrum GX). Samples

were diluted by KBr at a ratio of 1/300 (by weight) and pressed into pellets. The spectrum was averaged over five runs with a resolution of 1.0 cm^{-1} in the range of 400–4000 cm^{-1}.

FESEM and EDX characterizations

FESEM (JEOL JSM-6700F) was used to study the morphology of samples. Before observation, samples were coated with platinum at 20 mA for 100 s using a sputter (JEOL JFC-1600). The elements in each sample were characterized by EDX, which is coupled with FESEM.

ICP analysis

The concentrations of Mn or Fe, Ca and P elements in each sample were quantified by ICP (Prodigy-Teledyne Instruments Leeman Lab). ICP was calibrated by standard solutions of each element of interest and samples were prepared by dissolving 40 mg powder in 250 mL 1 wt% HNO_3.

Magnetic property test

The magnetic property of FeHA powder was studied at room temperature in the range of magnetic field 0–10 kOe using VSM (Lake Shore 7404).

Cell study

Pellets of metal ion substituted HA were prepared by pressing 120 mg powder in a 13 mm die (Specac®, PT. No. 3006 BDH) at 1 ton-load and autoclaved before use. Human fetal osteoblast cell line (hFOB 1.19) from American Type Culture Collections (ATCC) was cultured in Dulbecco's modified Eagle's medium/Ham's F12 (DMEM/F12) supplemented with 10% fetal bovine serum (FBS) in a humidified atmosphere of 5% CO_2 in air at 37 °C.

Cytotoxicity test

The cytotoxicity of all samples was tested using extraction assay. Cells were seeded on 24-well plates at a density of 5×10^4 cell/mL and incubated for 1 day. The medium in each well was then replaced by the extraction medium (4 replicates for each composition, 1 mL/well) and incubated for another 72 h. The extracted medium was obtained from 2.12 mL DMEM/F12 medium, which was used to incubate one pellet at 37 °C for 72 h. The cells cultured with DMEM/F12 medium acted as the control. Methyl thiazole tetrazolium (MTT) method was used to measure the viability of cells. The concentration of Fe in the extracted medium was measured in four replicates using colorimetric assay which was made use of Fe chelator. The absorbance was monitored at 538 nm [19].

Cell seeding

Cells were seeded on pellets at a density of 5×10^4 cell/pellet in 24-well plates (4 replicates for each composition). The wells without pellets were used as the controls. The culture medium was changed every 2 days and MTT method was applied to quantify the cell viability. The cell growth profile was investigated for 3 days and 7 days. For the interpretation of cell adhesion result, zeta potential of HA, Mn5 and Fe5 powder in DI water was assessed using Malvern Zetasizer Nano-ZS at 37 °C.

Cell morphology

Osteoblast cells on HA, Mn5 and Fe5 pellets were fixated after 3-day incubation (two replicates for each sample). The samples were first rinsed with phosphate buffer saline solution (PBS), followed by cell fixation in 0.1 M sodium cacodylate containing 2.5% glutaraldehyde at room temperature. After 45-min fixation, the samples were washed with 0.1 M sodium cacodylate. The cells were further fixed in 1% tannic acid for 30 min at 4 °C and rinsed in 0.1 M sodium cacodylate buffer. The samples were then dehydrated in a graded series of ethanol and subsequently hexamethyldisilazane. The cell morphology was observed under FESEM (JEOL JSM-6700F).

Statistical analysis

Differences between groups were analyzed using Student's t test and were considered statistically significant at $p \leq 0.05$.

Results

Pure HA, MnHA and FeHA nanoparticles were successfully synthesized using wet chemical method and ion exchange mechanism. Pure HA was white while the colors of MnHA and FeHA were pink and brown, respectively. As substitution concentration increased, the color intensity increased accordingly.

Structure and composition of metal ion doped HA

XRD analysis

To examine the lattice parameters and crystal size of the produced nanoparticles, we performed XRD analysis. The peaks on the XRD patterns (Fig. 1) agreed well with ICSD

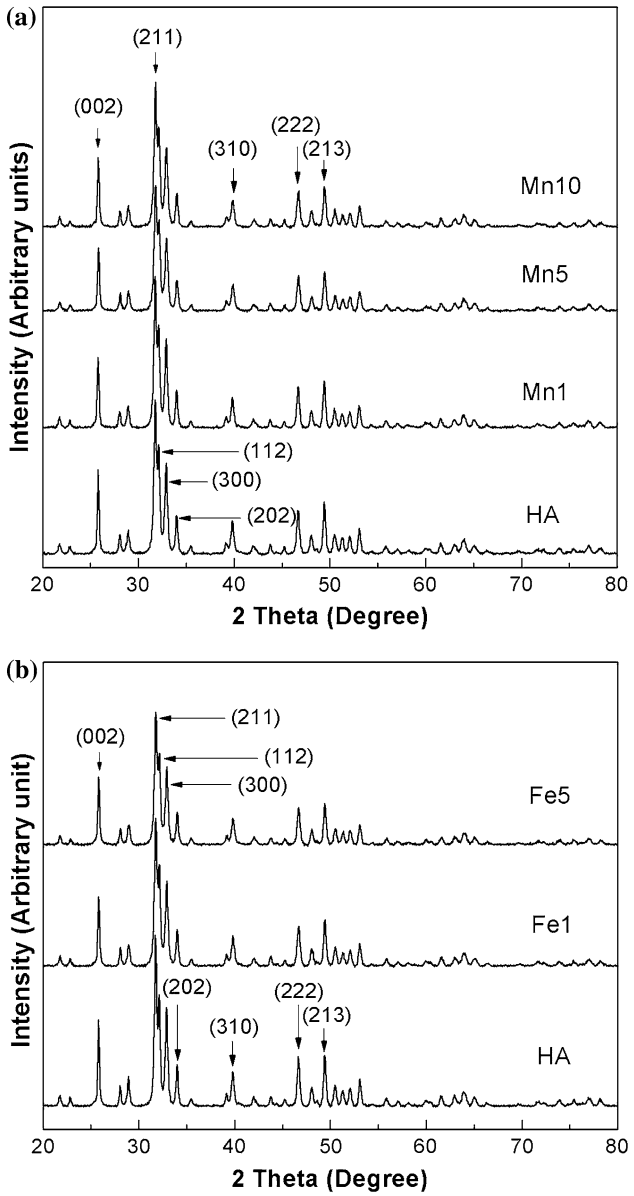

Fig. 1 XRD patterns of **a** MnHA powder and **b** FeHA powder compared to pure HA

file no. 26204 indicating that all samples were single phased hexagonal hydroxyapatite. Compared with pure HA, both MnHA and FeHA showed comparable peak positions without significant shift, regardless of substitution concentrations, which suggested that the lattice structure of HA were not markedly affected by the ion exchange process. The unit cell volume of MnHA was slightly smaller than that of pure HA while for FeHA, it was larger (Table 1). For MnHA, lattice parameters *a*, *c* and unit cell volume decreased with the increase of Mn content. As for FeHA, the lattice parameters and unit cell volume increased with the addition of Fe. The crystal size calculated based on Scherrer equation for MnHA and FeHA was comparable to that of pure HA.

Table 1 Lattice parameters and crystal size for all samples from XRD patterns

Sample	Lattice parameters			Crystal size (nm)
	a (Å)	*c* (Å)	Volume (Å^3)	
HA	9.4233(7)	6.8981(6)	530.48(9)	41
Mn1	9.4219(7)	6.9005(6)	530.50(9)	38
Mn5	9.4221(9)	6.8989(7)	530.40(11)	38
Mn10	9.4209(9)	6.8982(7)	530.22(11)	39
Fe1	9.4246(8)	6.9005(6)	530.80(10)	41
Fe5	9.4240(9)	6.9011(7)	530.78(11)	39

FTIR spectra

Figure 2 shows the FTIR spectra of pure HA, MnHA and FeHA nanoparticles. The detection of PO_4^{3-} and OH^- adsorption bands indicated that all samples possessed fundamental apatite structures [20]. In addition, carbonate CO_3^{2-} and water H_2O adsorption bands were noticeable within all spectra. Presence of hydrogen phosphate, such as HPO_4^{2-} and $H_2PO_4^-$, adsorption bands were not visible in all spectra.

FESEM and EDX characterizations

To assess the particle morphology and the presence of the elements of interest, the samples were subjected to FESEM and EDX characterizations. The FESEM images of pure HA, Mn5 and Fe5 are shown in Fig. 3. All samples had similar particle morphology, which was elongated spheroid of around 70 nm. The elements present in HA phase, such as C, O, P, Ca and Mn or Fe, were detected by EDX. Representative EDX spectra are shown as insets on Fig. 3. For both MnHA and FeHA, no Cl was detected.

ICP chemical analysis

Ca, P and Mn or Fe concentration in each sample was quantified using ICP. Ca/P, M/Ca and (Ca + M)/P atomic ratios from the ICP data were tabulated in Table 2. For pure HA, Ca/P atomic ratio was higher than the stoichiometric value of 1.667 [21], while for MnHA and FeHA, Ca/P ratio decreased and M/Ca ratio increased with the increase of initial metal ion concentration, indicating that more Ca ions in the lattice structure were replaced by the metal ions. For MnHA, Ca/P ratio from ICP data was higher than the theoretical value of Ca/P[a] and the Mn/Ca ratio was lower than the theoretical value, especially for Mn10. This indicated that not all Mn^{2+} ions added in the

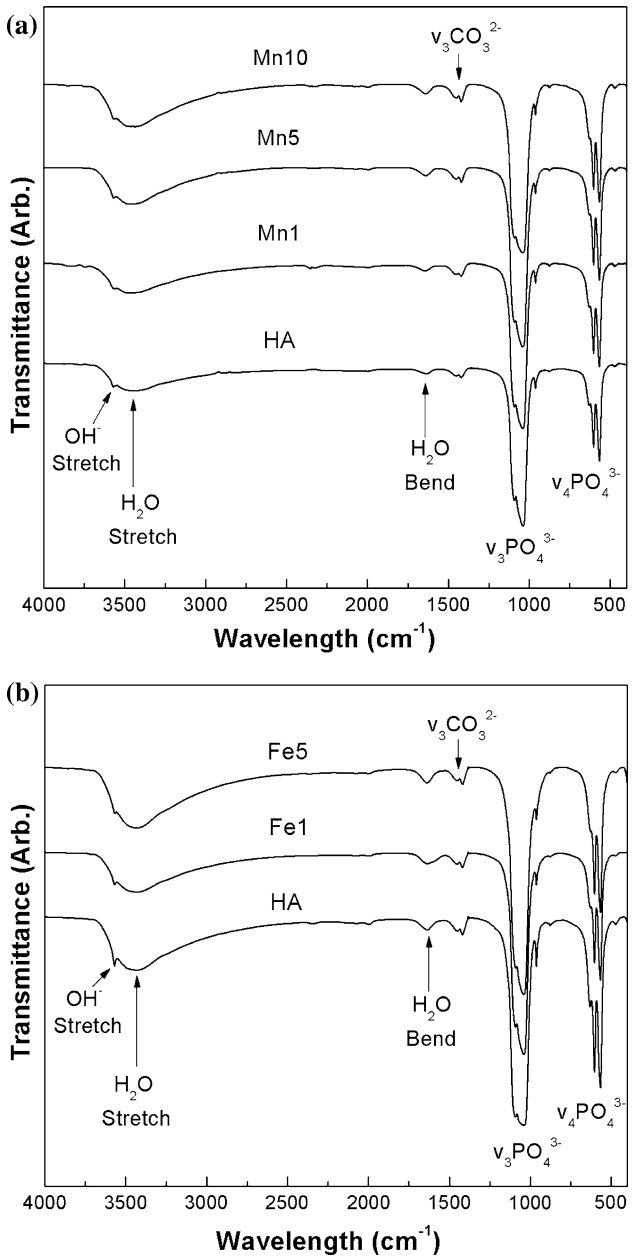

Fig. 2 FTIR spectra of **a** MnHA powder and **b** FeHA powder compared to pure HA

suspension were involved in the ion exchange process. As for FeHA, Ca/P ratio was higher than the theoretical value, suggesting that the exchange ratio of Fe/Ca was less than 3/2.

Magnetic property of FeHA

The magnetization of FeHA powder versus external magnetic field is shown in Fig. 4. Pure HA and Fe1 were diamagnetic as the magnetization was proportional and opposing to the applied magnetic field while Fe5 was paramagnetic since the magnetization increased linearly with the external field. The magnetic susceptibility (χ_g) of Fe5 was 9.25×10^{-7} emu g^{-1} Oe^{-1}.

Cell studies of metal ion doped HA

Cytotoxicity analysis

MTT test was used to examine cell viability after the cells were cultured in extraction medium for 72 h. The number of viable cells was calculated based on the absorbance value from MTT test. Compared with pure HA, Mn5, Mn10 and Fe5 have significantly more cells ($p < 0.05$) (Fig. 5).

The concentrations of Fe in the extracted medium were quantified using colorimetric assay. The values were 0.182 ± 0.071 ppm, 0.197 ± 0.000 ppm, 0.291 ± 0.047 ppm, 0.478 ± 0.047 ppm for DMEM/F12, HA, Fe1 and Fe5 extracted medium accordingly. The concentration of Fe in the extracted medium increased proportionally with Fe content in HA.

Cell proliferation on sample pellets

Mn5 and Fe5 were chosen for osteoblast growth test. Among MnHA samples, no significant difference was found in the cell numbers on Mn5 and Mn10 pellets after incubation for 7 days. However, Mn5 had 27% more cells than Mn1 after 7 days incubation (data not shown). As for FeHA, our results suggested strong dependence between cell number and Fe concentration. The cell number on Fe1 pellets was comparable to that of pure HA pellets while the number of cells found on Fe5 pellets was twice that of pure HA (data not shown). To verify the supposition, samples with higher Fe concentration (Fe10 and Fe15) were produced and cell adhesion was tested (data not shown). On day 3, the number of cells on these samples were significantly higher than on pure HA ($p < 0.05$), with Fe5 giving the highest cell number and chosen for further tests.

The cell growth profiles for pure HA, Mn5 and Fe5 were obtained, as shown in Fig. 6. Only Mn5 demonstrated marked cell proliferation from day 3 to day 7 ($p < 0.1$) while the cell number on both pure HA and Fe5 pellets did not increase significantly ($p > 0.05$) from day 3 to day 7. Compared with pure HA, Fe5 pellets had significantly more cells ($\sim 180\%$ higher) on both day 3 and day 7 ($p < 0.05$). Since Ohgaki et al. reported that negatively charged surface of electrically polarized HA promoted osteoblast-like cells growth in vitro [22], the zeta potential of pure HA, Mn5 and Fe5 in DI water at 37 °C was measured to assess the surface charge. The values were -0.91 ± 0.26 mV, -4.49 ± 0.30 mV and -11.65 ± 3.17 mV, respectively. Fe5 had the most negatively charged surface among the samples investigated.

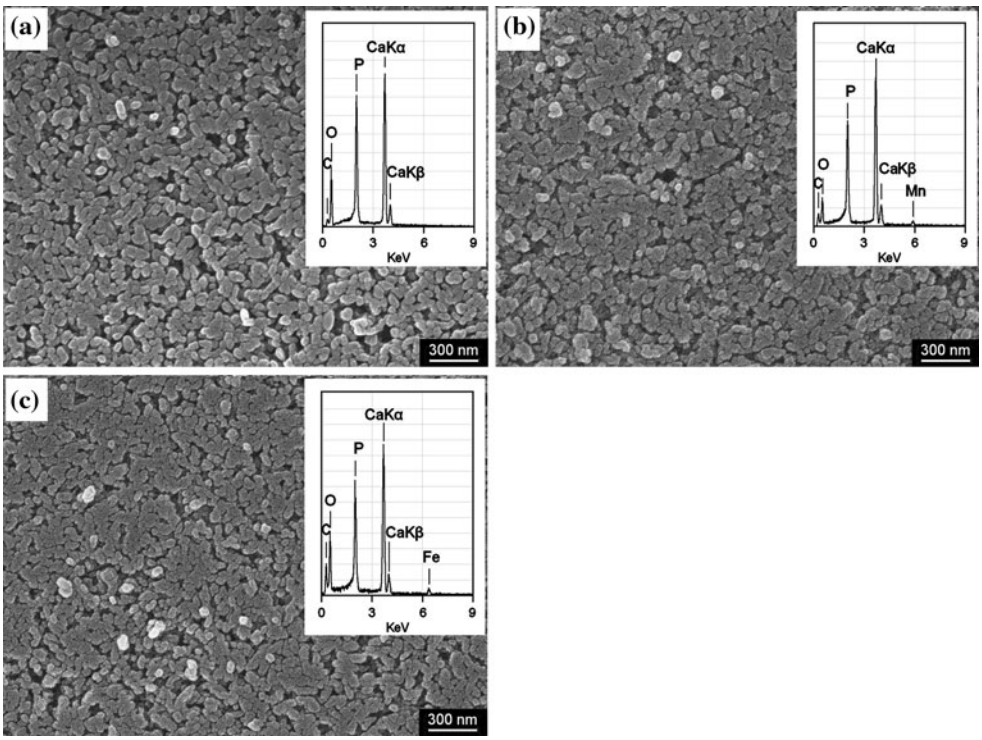

Fig. 3 Representative FESEM images of metal ion doped HA at 40,000× magnification. **a** pure HA, **b** Mn5 and **c** Fe5. Scale bar is 300 nm

Table 2 The atomic ratios for all samples from ICP data

Samples	Ca/P	Ca/P[a]	(Ca + M)/P	M/Ca	M/Ca[b]
HA	1.681	–	–	–	–
Mn1	1.660	1.664	1.675	0.010	0.010
Mn5	1.620	1.597	1.681	0.041	0.053
Mn10	1.599	1.513	1.683	0.053	0.111
Fe1	1.661	1.656	1.678	0.010	0.010
Fe5	1.589	1.555	1.677	0.055	0.054

[a] Theoretical atomic ratio of Ca to P after Ca was replaced by all the M ions added at the corresponding ratio. For Mn^{2+} doped HA, the assumed exchange ratio of Mn/Ca was 1:1 and for Fe^{3+} doped HA, the assumed exchange ratio of Fe/Ca was 3:2 to maintain the charge balance. The initial value of Ca/P[a] was derived from HA ICP result of 1.681

[b] Theoretical atomic ratio of M to Ca after replacement of Ca by all the metal ions added at the corresponding ratio

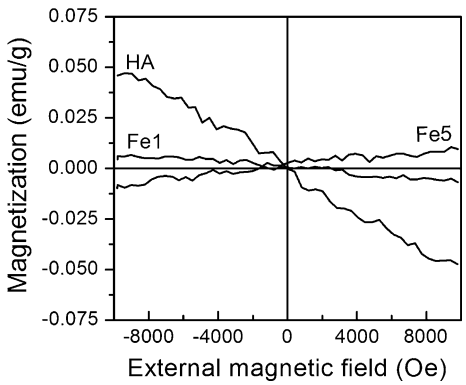

Fig. 4 Magnetization curves of FeHA powder measured at room temperature

Cell morphology analysis

Filopodia are important characteristic of osteoblast cells and their presence provides further confirmation of osteoblast attachment to sample pellets. Figure 7 shows the FESEM images of osteoblast cells growing on pure HA, Mn5 and Fe5 pellets for 3 days. On all surfaces, osteoblast cells spread well and grew actively. Compared with pure HA, cells on Mn5 pellets were more flattened and the cellular membrane was closer to the pellet surface, as if they were almost fused together. The osteoblast cells on Fe5 pellets showed more mini-filopodia (indicated by an arrow on Fig. 7c) than cells on both pure HA and Mn5 pellets.

Discussion

Metal ion doped HA was successfully synthesized by wet chemical method coupled with ion exchange mechanism. As confirmed by the characterization techniques, the metal ion doped HA was single phased, B-type carbonated and non-stoichiometric HA. As shown in Fig. 1, no extra peaks

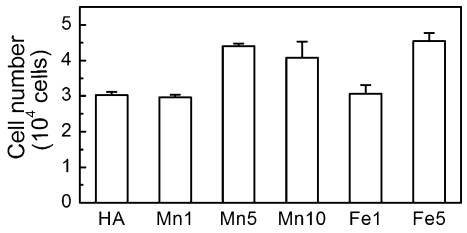

Fig. 5 Cell number based on MTT test for osteoblast cells cultured in extracted medium for 72 h. Data = mean + standard deviation; $n = 4$

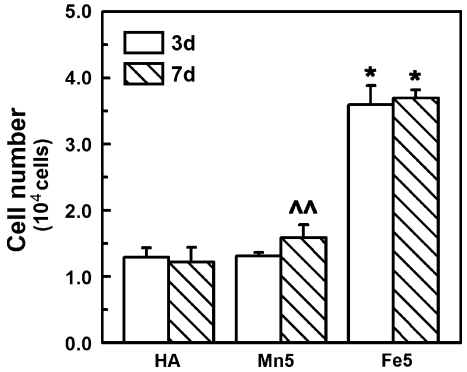

Fig. 6 Cell number based on MTT test for osteoblast cells growing on HA, Mn5 and Fe5 pellets for 3 and 7 days. Data = mean + standard deviation; $n = 4$; * $p < 0.05$ as compared to HA with the same incubation time; ^^ $p < 0.1$ as compared to 3-day incubation of the same sample

but those belonging to HA phase were present. Carbonate groups demonstrated noticeable adsorption bands besides the characteristic bands of HA in the FTIR spectra (Fig. 2), which might have originated from atmospheric carbon dioxide and/or $CaCO_3$ impurities in $Ca(OH)_2$. In HA lattice structure, carbonate groups can partially replace the PO_4^{3-} groups, giving rise to the B-type carbonated HA. The presence of carbonate was not expected to affect the cell response since it is naturally present in bones [7]. Meanwhile, CO_3^{2-} ions contributed to the higher Ca/P atomic ratio; 1.681 for pure HA compared to the theoretical Ca/P value of 1.667 (Table 2).

The lattice parameters of metal ion doped HA (Table 1) together with the peak positions in XRD patterns (Fig. 1) were comparable with that of pure HA, suggesting that ion exchange did not significantly alter the HA structure. Partial replacement of Ca^{2+} ions by other cations with smaller ionic radii will result in smaller lattice parameters a and c. Both Mn^{2+} (0.67 Å) and Fe^{3+} (0.65 Å) ions are of smaller ionic radii than Ca^{2+} ions (1.00 Å) [23]. Lattice parameters for MnHA decreased as Mn content in HA increased (Table 1). This observation was further supported by ICP results, where (Ca + M)/P atomic ratio of MnHA was comparable with Ca/P atomic ratio of pure HA, indicating that Mn^{2+} ions successfully replaced Ca^{2+} at the lattice positions.

In contrast, FeHA resulted in larger lattice parameters compared to those of pure HA (Table 1). This was probably due to partial replacement of Ca^{2+} with Fe^{3+} and Fe hydroxo ions ($Fe(OH)^{2+}$) as suggested by Wakamura et al. [14]. In our calculation, the exchange ratio of Fe/Ca was assumed to be 1.5 to maintain charge balance. However, the measured Ca/P ratios were higher than the theoretical values (Table 2), which suggested that the exchange ratio of Fe/Ca was less than 1.5. If the exchange ratio of Fe/Ca was 1, Ca/P ratios from ICP result should have been less than the theoretical values of 1.664 and 1.597 for Fe1 and Fe5, respectively. Hence, it can be concluded that the exchange ratio of Fe/Ca here was between 1 and 1.5. This observation was consistent with Wakamura et al. who estimated the exchange ratio of Fe/Ca as 1.3. Limited by sample number, the exchange ratio was not calculated here.

Compared with Mn^{2+} ions, Fe^{3+} ions were more active in replacing Ca^{2+} in HA lattice. As shown in Table 2, Mn/Ca atomic ratio was smaller than Fe/Ca atomic ratio for molar quantity (M_{added}/Ca_{added}) of 5% and above. The Ca/P atomic ratio for Mn5 was larger than Fe5 when the same molar quantity of metal ions was added during the fabrication process. Furthermore, Mn/Ca atomic ratio was less than the theoretical value for Mn5 while Fe/Ca for Fe5 was comparable with the theoretical value. This may be due to the different electron density (atomic valence per volume of ions) between Mn^{2+} and Fe^{3+} ions. Even though both ions had close ionic radii, they had different charges which influenced the efficiency in which the metal ions replaced Ca^{2+} in HA.

The magnetic property of FeHA was characterized as diamagnetic or paramagnetic by VSM. Fe5 was paramagnetic with magnetic susceptibility (χ_g) of 9.25×10^{-7} emu g^{-1} Oe^{-1} (saturation magnetization (M_s) at 10 kOe was 9.25×10^{-3} emu g^{-1}). Wu et al. [13] reported that Fe^{2+} substituted HA nanoparticles were superparamagnetic and the highest M_s was 20.92 emu g^{-1}. The significant difference was probably due to the fabrication techniques and valance of Fe ions used. Here, Fe^{3+} and ion exchange method was chosen while Wu et al. introduced Fe^{2+} ions into HA nanoparticle by coprecipitation method [13]. To date, the ferromagnetic and superparamagnetic properties of nanoparticles are preferred for biomedical applications such as drug delivery, contrast agents for magnetic resonance imaging (MRI) and heat mediators for hyperthermia treatment [13]. Our results suggested that the FeHA nanoparticles produced using ion exchange mechanism would not be suitable for such applications due to their low magnetic susceptibility and magnetization.

The extraction assay in the cytotoxicity test was to quantify the toxicity of water soluble chemicals from the

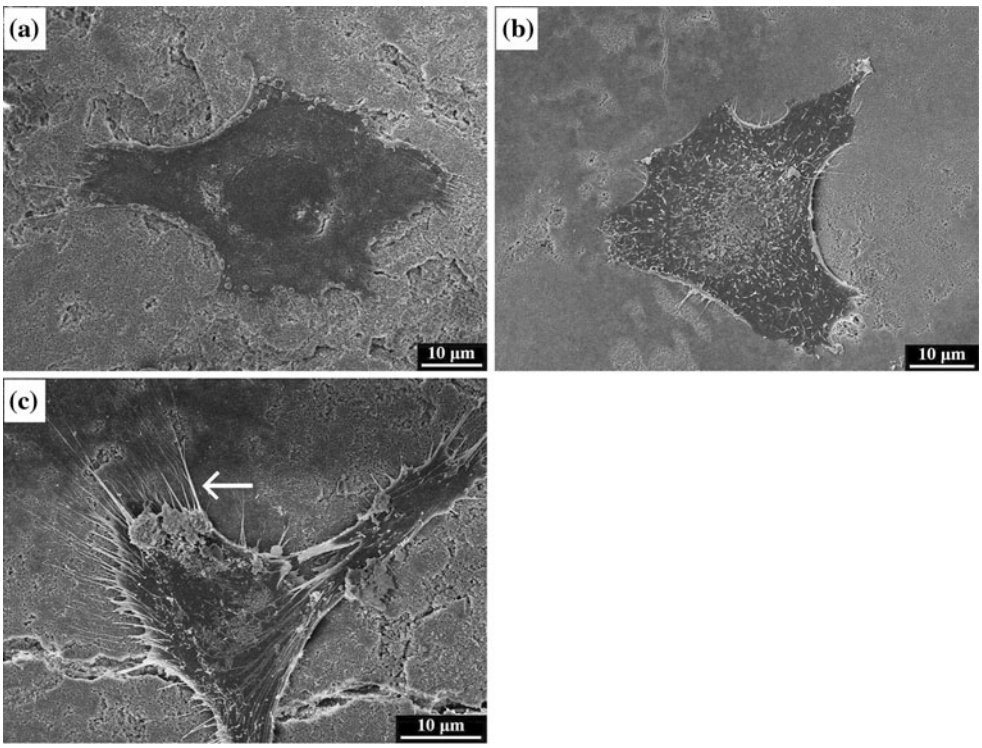

Fig. 7 Representative FESEM images of cells growing on sample pellets for 3 days. **a** pure HA, **b** Mn5 and **c** Fe5. Scale bar is 10 μm

specimens [24]. For single phased MnHA or FeHA, the possible water soluble components included Mn^{2+} or Fe^{3+} in addition to the dissolution products of pure HA such as Ca^{2+}, $PO_4{}^{3+}$ and OH^- ions. As shown in Fig. 5, the number of cells after 3 days incubation in the media extracted from MnHA or FeHA samples was comparable or higher than pure HA suggesting that doping with neither Mn nor Fe demonstrated toxicity to osteoblast cells.

In the extraction assay, we found that cell numbers in Mn5 and Fe5 extracted medium were much higher than in the extracted medium from pure HA. We further seeded osteoblast cells onto the pellets and observed the cell morphology using FESEM after incubating for 3 days. Cell density on Fe5 pellets appeared to be much higher than Mn5 and pure HA. Additionally, cells grew actively on Fe5 pellets and numerous newly divided cells were observed. Filopodia were also observed for cells on Fe5, which are regarded as one of the most important cellular sensors [25, 26] and with which epithelial cells would migrate [27]. These filopodia indicated good osteoblast attachment on Fe5 pellets. Adhesion of osteoblast to matrix is an important step for osteointegration which prevents motion-induced damage [8]. In order to quantify the biocompatibility of Fe5 as compared to pure HA, we conducted the proliferation studies of osteoblast cells on those pellets.

As shown in the growth profile of cells seeded on pure HA, Mn5 and Fe5 pellets (Fig. 6), only cells on Mn5 demonstrated slight proliferation from day 3 to day 7 ($p < 0.1$). The low proliferation rate of cells even on pure HA may be due to the poor mechanical property of cold pressed pellets without sintering. In other work, cell seeding was usually carried out on sintered HA pellets [8, 15, 21, 28, 29]. However, metal ion doped HA pellets were reported to show different grain size after sintering compared to pure HA [8, 30] and grain size affected osteoblast proliferation [15]. As reported by Webster et al. [15], osteoblast proliferation was significantly greater on nanophased HA (grain size 67 nm) than conventional HA (grain size 179 nm) after 3 and 5 days. Besides the change in grain size, sintering would also oxidize Mn^{2+} to Mn^{5+} [6], where the latter was no longer the ion of interest in this investigation. Hence, cold pressed pellets were used to keep the surface morphology of pellets comparable to each other (FESEM images, Fig. 3) and the valence of doped metal ion unchanged even though the pellets formed were brittle in nature. For future studies, binder material may be used to make the pellets more compact and hence, increase the mechanical strength.

After osteoblast seeded on MHA pellets, we observed significantly more cells on Fe5 pellets as compared to Mn5 and pure HA (from the MTT assay shown in Fig. 6). This notable different cell behavior on Fe5 pellets was probably due to the difference in surface charge of Fe5 as compared to pure HA and Mn5. A bonelike apatite layer is formed on

HA after soaking in simulated body fluid (SBF). The process is initiated by the formation of Ca-rich amorphous or nano-crystalline calcium phosphate due to the negatively charged surface of HA after exposure to SBF together with the higher bonding affinity with Ca^{2+} ions than other metal ions [31]. Yamashita et al. [32] showed that accelerated apatite growth was observed on negatively charged surface while no crystal grew on positively charged surface of HA, which suggested that negatively charged surface attracted the Ca^{2+} ions. Ohgaki and Kobayashi et al. reported that negatively charged surface of electrically polarized HA promoted colony formation of osteoblast-like cells in vitro [22] and the negatively charged HA conducted formation of bone layer much faster than conventional HA in vivo [33]. In our experiment, the zeta potential for Fe5 in DI water at 37 °C (-11.65 ± 3.17 mV) was more negative than that of Mn5 (-4.49 ± 0.30 mv) and pure HA (-0.91 ± 0.26 mV). The more negatively charged surface of Fe5 pellets would absorb more Ca^{2+} ions and eventually more osteoblast cells. The osteoblast cell adhesion initiated by Ca^{2+} adsorption, would further attract cell adhesion proteins, like vitronectin which promoted cell adhesion. Vitronectin is negatively charged in cell culture medium since its isoelectric point is 4.75–5.25 [34]. The fact that osteoblast cells preferred Fe5 pellets over pure HA pellets was also supported by cell morphology studies. Based on our results, Fe5 is a potential candidate for implants or coating materials which require good osteointegration.

Conclusion

Hydroxyapatite (HA) substituted with Mn^{2+} and Fe^{3+} was successfully synthesized by wet chemical method coupled with ion exchange mechanism. All samples were single phased without significant structure deviation and were B-type carbonated HA as carbonate groups partially replaced phosphate groups in the lattice structure. Since ion exchange mechanism was applied, the morphology and crystal size of Mn^{2+} substituted (MnHA) and Fe^{3+} doped HA (FeHA) nanoparticles were not significantly affected as compared to pure HA. With the increase of initial metal ion concentration, the quantity of metal ion in HA lattice increased accordingly. As suggested by inductively coupled plasma (ICP) data, Fe^{3+} ions were more active than Mn^{2+} ions in the exchange with Ca^{2+} ions in HA lattice. Fe5 was paramagnetic while pure HA was diamagnetic. Neither MnHA nor FeHA demonstrated toxic effect on osteoblast cells. Osteoblast adhesion enhancement was observed on FeHA, where the addition of Fe^{3+} ions in HA successfully increased the negative charge of pellets surface and osteoblast cell adhesion as compared to pure HA and MnHA.

Acknowledgements The authors wish to acknowledge Chai Teck Nam for preliminary work on the synthesis of MnHA and FeHA powders.

References

1. Oktar FN (2007) Ceram Int 33:1309
2. Klein CPAT, Patka P, Wolke JGC, de Blieck-Hogervorst JMA, de Groot K (1994) Biomaterials 15:146
3. Mihailescu IN, Torricelli P, Bigi A, Mayer I, Iliescu M, Werckmann J, Socol G, Miroiu F, Cuisinier F, Elkaim R, Hildebrand G (2005) Appl Surf Sci 248:344
4. Wieser E, Tsyganov I, Matz W, Reuther H, Oswald S, Pham T, Richter E (1999) Surf Coat Technol 111:103
5. Feng QL, Kim TN, Wu J, Park ES, Kim JO, Lim DY, Cui FZ (1998) Thin Solid Films 335:214
6. Mayer I, Jacobsohn O, Niazov T, Werckmann J, Iliescu M, Richard-Plouet M, Burghaus O, Reinen D (2003) Eur J Inorg Chem 2003:1445
7. György E, Toricelli P, Socol G, Iliescu M, Mayer I, Mihailescu IN, Bigi A, Werckman J (2004) J Biomed Mater Res A 71:353
8. Webster TJ, Massa-Schlueter EA, Smith JL, Slamovich EB (2004) Biomaterials 25:2111
9. Parelman M, Stoecker B, Baker A, Medeiros D (2006) Exp Biol Med (Maywood) 231:378
10. Sato K, Nohtomi K, Demura H, Takeuchi A, Kobayashi T, Kazama J, Ozawa H (1997) Bone 21:57
11. Takeuchi K, Okada S, Yukihiro S, Inoue H (1997) Pathophysiology 4:97
12. Guggenbuhl P, Filmon R, Mabilleau G, Basle MF, Chappard D (2008) Metabolism 57:903
13. Wu H-C, Wang T-W, Sun J-S, Wang W-H, Lin F-H (2007) Nanotechnology 18:165601
14. Wakamura M, Kandori K, Ishikawa T (2000) Colloids Surf A 164:297
15. Webster TJ, Ergun C, Doremus RH, Siegel RW, Bizios R (2000) Biomaterials 21:1803
16. Wakamura M, Kazuhiko K, Tatsuo I (1998) Colloids Surf A 142:107
17. Sudarsanan K, Yong RA (1969) Acta Crystallogr Sect B-Struct Sci 25:1534
18. Li ZY, Lam WM, Yang C, Xu B, Ni GX, Abbah SA, Cheung KMC, Luk KDK, Lu WW (2007) Biomaterials 28:1452
19. Ljones T, Burris RH (2002) Biochemistry 17:1866
20. Kumar R, Prakash KH, Cheang P, Khor KA (2004) Langmuir 20:5196
21. Ergun C, Liu H, Webster TJ, Olcay E, Yilmaz S, Sahin FC (2008) J Biomed Mater Res A 85:236
22. Ohgaki M, Kizuki T, Katsura M, Yamashita K (2001) J Biomed Mater Res 57:366
23. Richerson D (2005) Modern ceramic engineering: properties, processing, and use in design, 3rd edn. CRC Taylor & Francis
24. Zhao Y, Zhang Y, Ning F, Guo D, Xu Z (2007) J Biomed Mater Res B Appl Biomater 83:121
25. Gustafson T, Wolpert L (1961) Exp Cell Res 24:64
26. Wood W, Martin P (2002) Int J Biochem Cell Biol 34:726
27. Andersson A-S, Brink J, Lidberg U, Sutherland DS (2003) IEEE Trans NanoBiosci 2:49
28. Webster TJ, Ergun C, Doremus RH, Bizios R (2002) J Biomed Mater Res A 59:312
29. Webster TJ, Ergun C, Doremus RH, Siegel RW, Bizios R (2000) J Biomed Mater Res A 51:475
30. Ergun C, Webster TJ, Bizios R, Doremus RH (2002) J Biomed Mater Res A 59:305

31. Kim H-M, Himeno T, Kokubo T, Nakamura T (2005) Biomaterials 26:4366
32. Yamashita K, Oikawa N, Umegaki T (1996) Chem Mater 8:2697
33. Kobayashi T, Nakamura S, Yamashita K (2001) J Biomed Mater Res A 57:477
34. Preissner KT, Seiffert D (1998) Thromb Res 89:1